

# Spatially Confined Hybridization of Nanometer-Sized NiFe Hydroxides into Nitrogen-Doped Graphene Frameworks Leading to Superior Oxygen Evolution Reactivity

Cheng Tang, Han-Sen Wang, Hao-Fan Wang, Qiang Zhang,\* Gui-Li Tian, Jing-Qi Nie, and Fei Wei

Oxygen evolution reaction (OER) catalysis constitutes the bottleneck in water splitting for a sustainable hydrogen economy<sup>[1–5]</sup> and, more importantly, is coupled with various renewable energy systems such as solar cells, metal-air batteries, and fuel cells.<sup>[6–9]</sup> However, this multi-electron process ( $4\text{OH}^- \rightarrow 2\text{H}_2\text{O} + \text{O}_2 + 4\text{e}^-$ , in base) suffers significantly from sluggish kinetics and a high overpotential, which calls for high-performance catalysts for commercial applications and has stimulated intense research interest. To date, precious metal oxides, such as  $\text{IrO}_2$  and  $\text{RuO}_2$ , have been identified as the most active catalysts,<sup>[10]</sup> but their practical use is prohibited by their low abundance, high cost, and poor durability. Emerging as a family of outstanding alternatives, transition metal (Ni, Co, Fe, Mn, etc.) oxides and their derivatives have attracted great attention recently,<sup>[11–27]</sup> because of their remarkable catalytic activity, high stability, abundance, and environmentally benign character. In recent studies, various carbon nanomaterials, such as nitrogen-doped graphite,<sup>[28]</sup> carbon nanotubes,<sup>[29,30]</sup> graphene,<sup>[28,31–39]</sup> and carbon quantum dots,<sup>[40]</sup> were also introduced into the catalytic system as an active phase or a multifunctional framework with synergistic effects, thereby enhancing the performance.

Among the aforementioned catalysts, nickel-iron layered double hydroxide/nanocarbon (NiFe LDH/NC) complexes are regarded as the most promising alternatives. NiFe LDHs exhibit extraordinary inherent catalytic activity for OER, which is probably due to the physical and electronic structure modification as a result of the Fe incorporation into  $\alpha\text{-Ni}(\text{OH})_2/\gamma\text{-NiOOH}$  lattices. Recently, extensive efforts have been dedicated to the in-depth investigation of optimal metal ratios or structural phases, leading to higher activities, by means of either in situ spectroscopy or density functional theory calculation, in spite of the controversy over real active sites.<sup>[12,41–45]</sup> Besides, several hierarchical structures of NiFe LDHs<sup>[33,46,47]</sup> have been proposed and some kinds of nanocarbon substrates have been employed and strongly coupled<sup>[29,32,33,40,46]</sup> with NiFe LDHs to enhance the electrolyte-accessibility, gas-release, and electron-transport

characteristics. Notwithstanding these advances, however, the fine control of NiFe LDH hybridization into a specific substrate to obtain an increased electrochemically active surface area (ECSA), fully exposed active sites, and an optimal interfacial junction still remains a challenge on the way towards perfect NiFe LDH/NC systems.

With the aim of approaching this goal, we scrupulously designed a novel composite based on NiFe LDHs and graphene and facilely fabricated it, as described herein, in the quest for high-performance oxygen evolution electrocatalysis. As illustrated in **Figure 1a**, a nitrogen-doped graphene framework (NGF) was employed as a mesoporous substrate for the in situ growth and decoration of nanometer-sized NiFe LDHs (nNiFe LDHs). The nitrogen dopant and topology-induced defects of graphene contributed to the adsorption and anchoring of metal cations, and then the in-plane mesopores served as nanoreactors for spatially confined nucleation and growth of nNiFe LDHs, thereby resulting in a strong affinity and uniform dispersion of the as-grown nNiFe LDHs in the mesoporous graphene framework (**Figure 1b**). As a consequence, this hierarchical structure, with mesoporous channels, interconnected electron highway, intimate interfacial coupling, suppressed particle aggregation, and fully exposed active sites, was demonstrated to outperform a commercial Ir/C catalyst, with significantly higher activities, improved kinetics, and enhanced durability for oxygen evolution in alkaline conditions.

A mesoporous graphene framework with moderate defects is the prerequisite factor for the controllable decoration of nNiFe LDHs into nanocarbon scaffolding. In the work presented in this Communication,  $\text{Mg}(\text{OH})_2$ -derived MgO flakes were adopted as mesoporous catalysts for the templated growth of NGFs. Scanning electron microscopy (SEM) images indicated that the NGF obtained after the removal of templates still maintained a hexagonal appearance, like MgO, with a uniform lateral size of ca. 2  $\mu\text{m}$  and a thickness of ca. 50 nm (**Figure 2a**, **Figure S1** in the Supporting Information). Notably, the whole graphene layer was crinkled and folded regularly to form a honeycomb-like framework (**Figure S2a**, Supporting Information), of which the graphene nanocages with a size of 5–10 nm were originally occupied by MgO nanocubes (**Figure S2b,c**). Raman spectroscopy revealed that the intensity ratio of D to G bands ( $I_{\text{D}}/I_{\text{G}}$ ) of NGF was ca. 2.07 (**Figure S3**, Supporting Information), indicating a considerable number of defective sites, which were probably generated at the corners or edges of graphene nanocages owing to the nitrogen-doping and the novel topology.

C. Tang, H.-S. Wang, H.-F. Wang, Prof. Q. Zhang,  
Dr. G.-L. Tian, Dr. J.-Q. Nie, Prof. F. Wei  
Beijing Key Laboratory of Green Chemical Reaction  
Engineering and Technology  
Department of Chemical Engineering  
Tsinghua University  
Beijing 100084, P. R. China  
E-mail: zhang-qiang@mails.tsinghua.edu.cn



DOI: 10.1002/adma.201501901

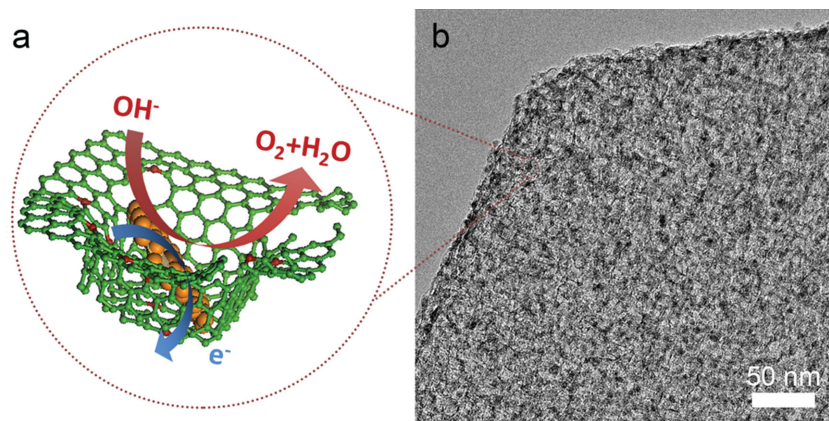


**Figure 1.** a) Schematic of the spatially confined hybrids. Nanometer-sized NiFe LDHs strongly associate with the nitrogen-doped graphene framework, with defect-anchored nucleation and spatially confined growth. Carbon atoms are indicated in green and nitrogen in red. b) Cross-sectional TEM image of a sheet of nNiFe LDH/NGF electrocatalyst.

These defective sites tended to adsorb and anchor metal cations in a nickel nitrate and iron nitrate solution (with a molar ratio of Ni/Fe = 3). As the precipitation proceeded, the nucleation and growth of NiFe LDH crystals were spatially confined by the graphene nanocages. Both SEM and transmission electron microscopy (TEM) images revealed that abundant NiFe LDH nanocrystals were selectively and uniformly decorated into the graphene scaffold (Figure 2b–d) without any obvious aggregation. The dark-field TEM image (Figure 2e) and energy dispersive spectroscopy (EDS) mapping (Figure 2f) also confirmed a uniform distribution of nNiFe LDHs over the whole graphene framework. High-resolution TEM images (Figure 2g)

showed that the NiFe LDH nanoplates exhibited a size of typically ca. 5 nm, and were divided from each other by encircling graphene layers. Further, the X-ray diffraction (XRD) pattern (Figure 3a) revealed that the nNiFe LDHs in the as-obtained composites were well crystallized, with a set of hydroxal-cite-like characteristic 003, 006, 012, and 110 peaks, representing a  $R\bar{3}m$  symmetry and hexagonal lattice, which is consistent with the lattice fringes shown in Figure 2g. The new Raman bands appeared at ca. 460 and 545  $\text{cm}^{-1}$ , which were associated with the  $\text{Fe}^{3+}/\text{Ni}^{2+}-\text{O}-\text{Ni}^{2+}$  and  $\text{Fe}^{3+}-\text{O}-\text{Fe}^{3+}$  linkage bands,<sup>[12,45]</sup> respectively (Figure S3), also revealed the incorporation of NiFe LDHs into the graphene framework. The atomic ratio of Ni to Fe was measured to be ca. 3.0 by X-ray photoelectron spectroscopy (XPS) (Figure 3b), EDS, and inductively coupled

plasma optical emission spectrometry, and was identical to that of their nitrate precursors (Table S1, Supporting Information). Note that this catalyst composition was in the optimal range for NiFe oxides/hydroxides as OER catalysts.<sup>[12,41,44]</sup> A counterpart hybrid using an undoped graphene framework (nNiFe LDH/GF) was also fabricated under otherwise identical conditions (Figure S4, Supporting Information). Nanometer-sized LDHs were observed in the pores of the undoped graphene framework, while some aggregates were also present. This indicated the importance of nitrogen dopants for an effectively anchored nucleation and improved dispersion of NiFe LDHs. Remarkably, the in situ grown nanometer-sized NiFe LDHs of nNiFe

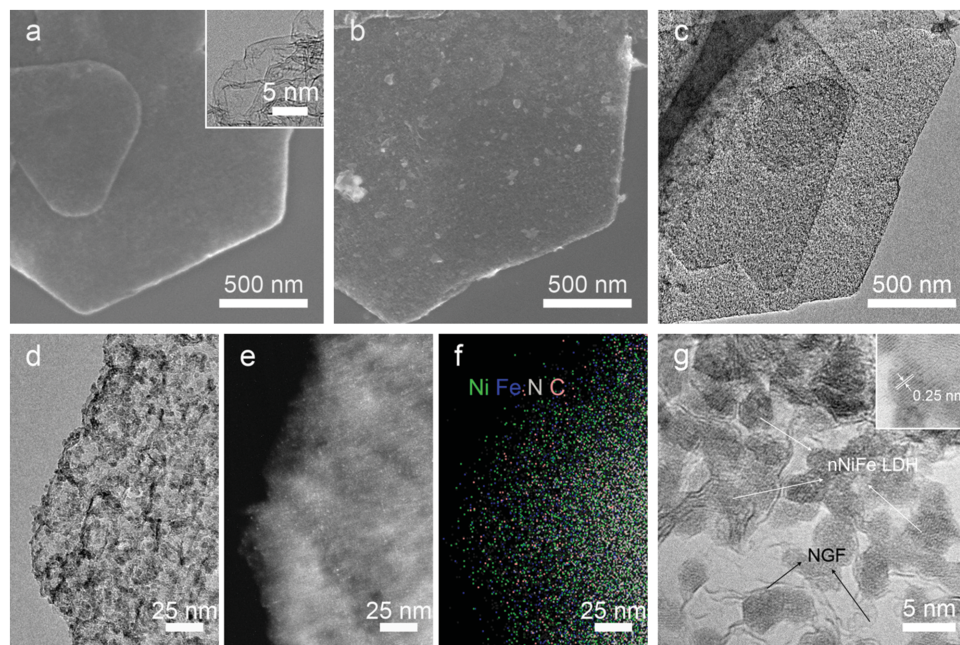


**Figure 2.** a–g) Morphology of nNiFe LDH/NGF electrocatalysts. a) SEM and TEM (inset) images of NGF sheets. SEM (b) and TEM (c) images of nNiFe LDH/NGF sheets exhibiting a uniform decoration of nNiFe LDHs into the graphene framework. TEM image (d), the corresponding dark-field TEM image (e), and EDS mapping (f) of nNiFe LDH/NGF electrocatalysts. g) TEM image and high-resolution TEM image (inset) of nNiFe LDH/NGF electrocatalysts.

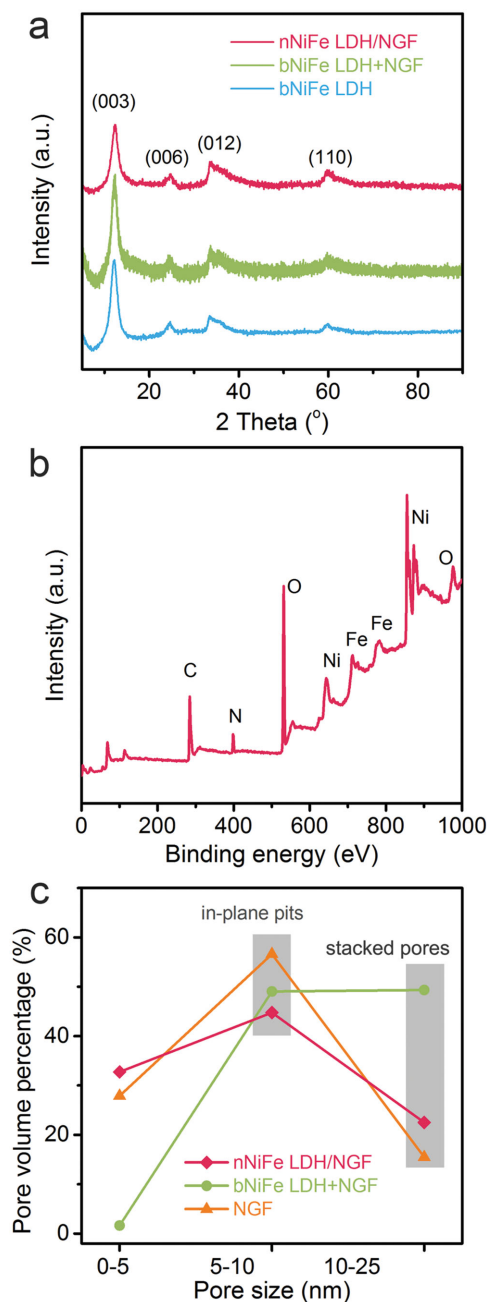


**Figure 3.** a–c) Structural characterization of nNiFe LDH/NGF electrocatalysts. a) XRD spectra of nNiFe LDH/NGF, bNiFe LDH, and physical mixture of bNiFe LDH and NGF. b) XPS survey spectrum of nNiFe LDH/NGF electrocatalysts. c) Pore size distribution comparison of NGF with in situ grown LDHs and mixed LDHs.

LDH/NGF exhibited the smallest size and best dispersion reported so far.

A physical mixture of bulk NiFe LDHs and NGF (bNiFe LDH+NGF) was fabricated for comparison, with the same mass ratio of nNiFe LDH/NGF as revealed by thermogravimetric analysis (TGA) (Table S1 and Figure S5 in the Supporting Information). The resultant composites, however, appeared to be quite different from the in situ grown nNiFe LDH/NGF.

Those NiFe LDH flakes synthesized without NGF substrates exhibited a much larger size and tended to aggregate into large clusters with a size of several hundred nanometers (Figure S6a, Supporting Information). Besides, the mesoporous graphene framework was nearly transparent under TEM owing to the absence of LDHs in the graphene cages (Figure S6b). This was further confirmed by the markedly distinct porous features of different samples (Figure 3c; Figure S7 in the Supporting Information). The pore sizes were characterized by  $N_2$  adsorption/desorption experiments and calculated based on quenched solid density function theory. Those mesopores with a size ranging from 5 to 10 nm were obviously more decreased for the in situ grown composites than for the mixtures, which was ascribed to the location of nNiFe LDHs in the in-plane pits of graphene frameworks. In the case of the physically mixed counterpart, the stacked pores larger than 10 nm were dramatically increased by ca. 33.8%. This was contributed by the LDH aggregation on and between graphene flakes.

The above-mentioned characterizations suggested the successful synthesis of a novel composite with nNiFe LDHs uniformly hybridized into a mesoporous graphene skeleton. The formation of unique nNiFe LDH/NGF electrocatalysts was a result of the introduction of the NGF substrate for a defect-anchored nucleation and spatially confined growth of nNiFe LDHs, which gave rise to fully exposed and accessible active sites and strongly coupled interfaces, thereby making the novel hybrid a superior candidate for OER electrocatalysis.

The water oxidation electrocatalytic performance of nNiFe LDH/NGF was first investigated in alkaline solution (0.10 M KOH) in a standard three-electrode setup with a loading of ca.  $0.25 \text{ mg cm}^{-2}$ . Individual components (bNiFe LDH and NGF), their physical mixture, and a commercial Ir/C catalyst were also tested for comparison. **Figure 4a** records the  $iR$ -corrected linear sweep voltammetry (LSV) curves at a scan rate of  $5.0 \text{ mV s}^{-1}$ . The redox peaks around 0.2 V overpotential were assigned to the  $Ni^{2+}/Ni^{3+}$  redox process (Figure S8, Supporting Information). The nNiFe LDH/NGF hybrid displayed a similar onset potential but substantially higher current density than the Ir/C catalyst, showing its remarkable activity. The high current density was demonstrated to result from the oxygen evolution process by rotating ring-disk electrode voltammetry measurements (Figure S9, Supporting Information). The horizontal dotted line in Figure 4a indicates the overpotential required to achieve a current density of  $10 \text{ mA cm}^{-2}$ , corresponding to 10% efficient solar water-splitting devices, which was adopted as a critical figure of merit for OER catalysts.<sup>[8,13]</sup> On this basis, the nNiFe LDH/NGF indeed outperformed the precious Ir/C catalyst with a 73 mV decreased overpotential for  $10 \text{ mA cm}^{-2}$  (ca. 337 mV) and dramatically surpassed both components and physical mixtures, a contribution of the synergistic and strong couple effects as a result of the novel structural features.

The outstanding catalytic activity was also reflected by Tafel slopes according to the Tafel equation  $\eta = b \log(j/j_0)$ , where  $\eta$  is the overpotential,  $b$  the Tafel slope,  $j$  the current density, and  $j_0$  the exchange current density. In our experiments, the current density  $j$  was obtained at specific potentials slightly above the  $Ni^{2+}/Ni^{3+}$  redox potential to decouple the redox and OER currents (Figure S10, Supporting Information). As shown in Figure 4b, the nNiFe LDH/NGF catalyst exhibited the lowest

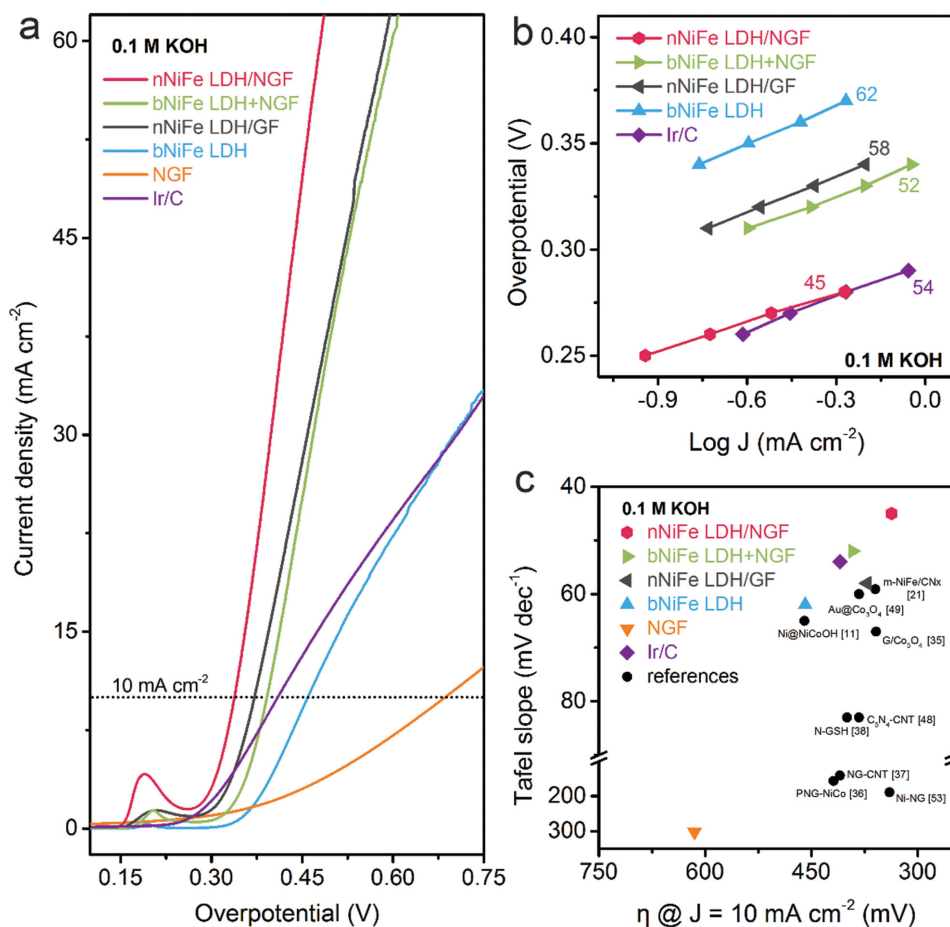


**Figure 4.** a–c) Oxygen evolution catalysis performances of nNiFe LDH/NGF and control samples in 0.1 M KOH electrolyte. a) LSV curves. Scan rate was 5.0 mV s<sup>-1</sup>. The loading was about 0.25 mg cm<sup>-2</sup> for all samples. b) Tafel plots of nNiFe LDH/NGF and other samples for comparison. c) Figures of merit with respect to both kinetics (Tafel slope) and activity (the overpotential required to achieve 10 mA cm<sup>-2</sup>), with references all measured in 0.1 M KOH electrolyte.<sup>[11,21,35–38,48,49,53]</sup>

Tafel slope of  $b \approx 45$  mV dec<sup>-1</sup>, while those of bNiFe LDH, physical mixture, and Ir/C catalysts were 62, 52, and 54 mV dec<sup>-1</sup>, respectively. Consequently, the lower Tafel slope of nNiFe LDH/NGF led to a greatly boosted current density at a higher overpotential, with a current density of 60 mA cm<sup>-2</sup> obtained at  $\eta \approx 480$  mV, which was nearly four-fold that of the Ir/C catalyst.

Taking the overpotential required for 10 mA cm<sup>-2</sup> and the Tafel slope  $b$  as two catalytic performance metrics, we comprehensively compared the nNiFe LDH/NGF catalyst with other similar catalysts and references with regard to both activity and kinetics (Figure 4c).<sup>[11,21,35–38,48,49]</sup> It is graphically represented that the novel nNiFe LDH/NGF hybrids exhibited a lower overpotential than most reported graphene and non-precious metal-based materials (in 0.10 M KOH) and are among the most kinetically active candidates for the water-splitting process (Table S2, Supporting Information).<sup>[48–51]</sup>

For a heterogeneous electrocatalytic process such as OER, the electrical conductivity, structural porosity, active sites, and interfacial coupling of the employed catalysts are the chief critical factors for the corresponding performances. In the case of nNiFe LDH/NGF, there is no doubt that the intrinsic merits of both components contribute greatly to the outstanding activity.

On one hand, the NGF affords a highly conductive and unique mesoporous scaffold with moderately active sites. A high conductivity of ca. 5400 S m<sup>-1</sup> was determined using the four-probe technique for NGF itself, while the bNiFe LDHs were demonstrated to be nearly non-conductive (ca. 10<sup>-8</sup> S m<sup>-1</sup>) (Figure S11, Supporting Information). Notably, for the in situ fabricated nNiFe LDH/NGF, a considerable conductivity of ca. 145 S m<sup>-1</sup> was maintained, hence ensuring a facile electron pathway. In addition, the highly porous framework delivered a large accessible surface and vast stacked interstices even after the LDH decoration, with a considerable specific surface area of 240 m<sup>2</sup> g<sup>-1</sup> and a total pore volume of 0.30 cm<sup>3</sup> g<sup>-1</sup>, thereby providing free channels for electrolyte ion insertion/extraction and gas diffusion (Figure S7). Furthermore, nitrogen incorporation into carbon frameworks is demonstrated to tailor the electronic structure of the adjacent carbon atoms,<sup>[52]</sup> which provides a facilitated chemisorption of OH<sup>-</sup> species and additional activity for OER.<sup>[28,30,37,38,53]</sup> The NGF and nNiFe LDH/NGF both exhibited a remarkably enhanced electrochemical activity compared to their undoped counterparts (Figure S12, Supporting Information).

On the other hand, the introduction of nNiFe LDHs effectively moderated the surface character and created abundant highly active sites. The nNiFe LDH/NGF hybrid was much more hydrophilic with a contact angle of  $55.7^\circ$ , in contrast to  $72.0^\circ$  for the NGF without LDHs, which importantly facilitated the affinity between the catalyst and electrolyte and enhanced the permeation of electrolyte ions (Figure S13, Supporting Information). Remarkably, the bNiFe LDH catalyst itself delivered a low Tafel slope ( $62 \text{ mV dec}^{-1}$ ), demonstrating that the NiFe LDH catalyst is among the most promising alternatives for OER catalysis, which is consistent with previous reports.<sup>[12,19,29,32–34,43,44,46,47]</sup> To elucidate the intrinsic high activity, the substitution of  $\text{Fe}^{3+}$  was proposed to exert a partial-charge-transfer activation effect on the surrounding  $\text{Ni}^{3+}$  sites, thereby altering their local environment and average oxidation state with increased activities of  $\text{Ni}^{3+}$  sites.<sup>[12,43]</sup> Other reports, however, hypothesize that the  $\text{Fe}^{3+}$  incorporation generates more favorable active sites instead of  $\text{Ni}^{3+}$ ,<sup>[24,44,46]</sup> which is likely due to the near optimal adsorption of intermediates induced by the shorter Fe–O bonds in edge-sharing  $[\text{MO}_6]$  octahedra.<sup>[44]</sup>

Notably, in spite of the intrinsic merits of NiFe LDHs and the graphene framework, both nNiFe LDH/NGF and bNiFe LDH/NGF still delivered higher overpotential and Tafel slopes than nNiFe LDH/NGF (Figure 4), which implied that the dramatically enhanced catalysis performance did not merely arise from the mixing of excellent members, but was also dependent on its indispensable structural features.

With a further analysis of the  $\text{Ni}^{2+}/\text{Ni}^{3+}$  redox behaviors for different samples, it was noted that the peak areas varied considerably (Figure 5a; Table S3 in the Supporting Information). The peak areas were integrated and assigned to the total charge transferred to determine the extent of the  $\text{Ni}(\text{OH})_2/\text{NiOOH}$  transformation, as shown in the inset of Figure 5a. Normalized on the basis of bNiFe LDHs, this result revealed that the ratio of oxidized Ni was dramatically increased for nNiFe LDH/NGF hybrid and also increased several-fold in the case of other complexes, suggesting an enhanced  $\text{Ni}(\text{OH})_2/\text{NiOOH}$  transformation of NiFe LDHs. The resultant NiOOH phase after  $\text{Ni}^{2+}/\text{Ni}^{3+}$  redox is believed to be crucial to the active sites of NiFe LDHs for OER,<sup>[12,44]</sup> which is supported by the negative correlation between the extent of  $\text{Ni}^{2+}/\text{Ni}^{3+}$  redox and the overpotential required for a current density of  $10 \text{ mA cm}^{-2}$  (Figure 4a). Besides, the high-resolution Ni 2p spectra of nNiFe LDH/NGF exhibited a ca. 0.7 eV shift to higher binding energy compared with bNiFe LDHs, which indicated a modified local electronic structure of Ni cations, likely due to the binding between nNiFe LDHs and graphene, that is, C–N–Ni–O (Figure 5b). Therefore, it can be concluded that the strong coupling between NiFe

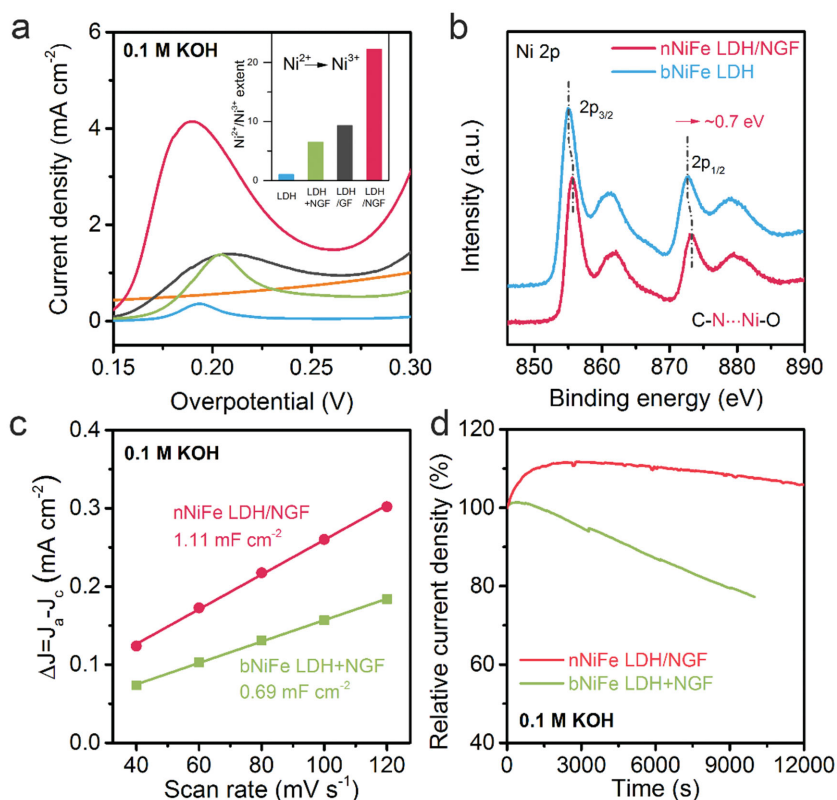


**Figure 5.** a–d) Enhanced oxygen evolution catalysis performances arising from the novel structural features. a) Enlargement of the  $\text{Ni}^{2+}/\text{Ni}^{3+}$  redox range in LSV curves. Inset: The normalized transformation ratio of  $\text{Ni}^{2+}$  on the basis of bNiFe LDHs. Legends are the same as Figure 4a. b) High-resolution Ni 2p spectra of nNiFe LDH/NGF and bNiFe LDHs, showing a ca. 0.7 eV shift to higher binding energy. c) Charging current density differences plotted versus scan rate. The linear slope, equivalent to twice the double-layer capacitance  $C_{dl}$ , was used to represent the ECSA. d) Chronoamperometric response at an overpotential of 350 mV.

LDHs and the graphene framework tuned the redox behavior of the Ni cations, leading to the resultant active phases in the OER process with better catalytic activities. Additionally, the strong interfacial bonding facilitated a rapid charge transfer, as evidenced by the lower Tafel slopes.

The physical mixture bNiFe LDH+NGF also exhibited a considerable interfacial coupling due to the nitrogen-doping-induced functional groups on graphene (Figure S14, Supporting Information), while the catalytic performances were greatly inferior to those of the in situ fabricated nNiFe LDH/NGF. This was elucidated by ECSA of the materials, which was estimated from the electrochemical double-layer capacitance ( $C_{dl}$ ) (Figure 5c). The ECSA of nNiFe LDH/NGF was 60% higher than that of bNiFe LDH+NGF, which was attributed to the smaller size and enhanced dispersion of NiFe LDHs with fully exposed and easily accessible active sites owing to the spatial confinement. The stability of both catalysts was tested at a constant overpotential of 350 mV. Figure 5d shows that the response current density of nNiFe LDH/NGF first increased and then stabilized, which was ascribed to the gradual infiltration of electrolyte into the porous catalyst and more accessible active sites during the OER process, while for bNiFe LDH+NGF it gradually decreased to a value of ca. 77% after 10000 s. The TEM image and XPS spectra of nNiFe LDH/NGF

after long-term cycling (Figure S15a-c, Supporting Information) reveal that the spatially confined morphology and physical structures are well preserved even after 12000 s catalysis, indicating a superior structural stability and thereby an enhanced durability. The remarkably enhanced durability of nNiFe LDH/NGF electrocatalyst was attributed to both the strong interfacial adherence and nanopore-confined effect for the stability of nNiFe LDH in the graphene framework.

Spatial confinement was introduced in order to achieve tunable growth and decoration of nanometer-sized NiFe LDHs into nitrogen-doped graphene frameworks. The superior OER catalytic performance of nNiFe LDH/NGF, as evidenced by a remarkably decreased overpotential (ca. 337 mV required for 10 mA cm<sup>-2</sup>), lower Tafel slope (ca. 45 mV dec<sup>-1</sup>), and enhanced stability, indicated that the proposed ubiquitous structure was favorable for superior electrocatalysis. First, the employed NGF substrate exhibited a high electrical conductive (ca. 5400 S m<sup>-1</sup>) and mesoporous architecture, which facilitated the electron transfer and mass diffusion during the OER process. Second, the uniformly decorated nNiFe LDHs moderated the character of the surface with an enhanced hydrophilicity for facile electrolyte permeation and introduced high intrinsic catalytic activities. Additionally, the strongly coupled interfaces arising from defect-anchored nucleation contributed to a modification of working active sites and a rapid interfacial charge transfer, leading to enhanced kinetics (Tafel slope  $\approx$  45 mV dec<sup>-1</sup>). Furthermore, the spatially confined growth and decoration ensured the resultant NiFe LDHs were nanometer sized and well dispersed, thereby generating more open coordination sites on the lengthened edge and a fully accessible active surface, which consequently stimulated the OER process. Taken together, the synergetic effect of two excellent components and the unique structural features of this novel nNiFe LDH/NGF hybrid make it an attractive alternative for OER electrocatalysis.

In summary, a novel NiFe LDH/graphene hybrid has been proposed and fabricated by means of defect-anchored nucleation and spatially confined growth of nanometer-sized NiFe LDHs into a three-dimensional graphene framework. Its excellent performance was attributed to its unique structural features and a synergetic effect; nNiFe LDH/NGF was demonstrated to outperform commercial Ir/C catalysts and compete favorably against reported alternatives for high-performance OER catalysis, with a remarkably low Tafel slope (ca. 45 mV dec<sup>-1</sup>), a substantially decreased overpotential (ca. 337 mV required for 10 mA cm<sup>-2</sup>), and enhanced durability. This strongly coupled complex is expected to be inspiring and applicable in various applications, such as heterogeneous catalysis, sensors, and energy conversion and storage. More importantly, the topology-assisted design and fabrication strategy opens up new avenues and sheds light on a novel branch of advanced nano-architected materials, thereby facilitating the wise hybridization of excellent components for specific applications.

## Supporting Information

Supporting Information is available from the Wiley Online Library or from the authors.

## Acknowledgements

C.T., H.S.W., and H.F.W. contributed equally to this work, which was supported by funding from the Natural Scientific Foundation of China (21306102 and 21422604) and Tsinghua University Initiative Scientific Research Program (20141081231 and 2014z22076).

Received: April 21, 2015

Revised: June 8, 2015

Published online:

- [1] J. A. Turner, *Science* **2004**, *305*, 972.
- [2] J. L. Fillol, Z. Codolà, I. Garcia-Bosch, L. Gómez, J. J. Pla, M. Costas, *Nat. Chem.* **2011**, *3*, 807.
- [3] I. Katsounaros, S. Cherevko, A. R. Zeradjanin, K. J. J. Mayrhofer, *Angew. Chem. Int. Ed.* **2014**, *53*, 102.
- [4] H. Dau, C. Limberg, T. Reier, M. Risch, S. Roggan, P. Strasser, *ChemCatChem* **2010**, *2*, 724.
- [5] Y. Jiao, Y. Zheng, M. Jaroniec, S. Z. Qiao, *Chem. Soc. Rev.* **2015**, *44*, 2060.
- [6] T. Maiyalagan, K. A. Jarvis, S. Therese, P. J. Ferreira, A. Manthiram, *Nat. Commun.* **2014**, *5*, 3939.
- [7] H. Wang, Y. Yang, Y. Liang, G. Zheng, Y. Li, Y. Cui, H. J. Dai, *Energy Environ. Sci.* **2012**, *5*, 7931.
- [8] M. G. Walter, E. L. Warren, J. R. McKone, S. W. Boettcher, Q. Mi, E. A. Santori, N. S. Lewis, *Chem. Rev.* **2010**, *110*, 6446.
- [9] T. Y. Ma, J. Ran, S. Dai, M. Jaroniec, S. Z. Qiao, *Angew. Chem. Int. Ed.* **2015**, *54*, 4646.
- [10] Y. Lee, J. Suntivich, K. J. May, E. E. Perry, Y. Shao-Horn, *J. Phys. Chem. Lett.* **2012**, *3*, 399.
- [11] Z. L. Zhao, H. X. Wu, H. L. He, X. L. Xu, Y. D. Jin, *Adv. Funct. Mater.* **2014**, *24*, 4698.
- [12] M. W. Louie, A. T. Bell, *J. Am. Chem. Soc.* **2013**, *135*, 12329.
- [13] C. C. L. McCrory, S. Jung, J. C. Peters, T. F. Jaramillo, *J. Am. Chem. Soc.* **2013**, *135*, 16977.
- [14] M. S. Burke, M. G. Kast, L. Trotochaud, A. M. Smith, S. W. Boettcher, *J. Am. Chem. Soc.* **2015**, *10*, 3638.
- [15] A. Grimaud, K. J. May, C. E. Carlton, Y. Lee, M. Risch, W. T. Hong, J. Zhou, Y. Shao-Horn, *Nat. Commun.* **2013**, *4*, 2439.
- [16] Y. Yang, H. L. Fei, G. D. Ruan, C. S. Xiang, J. M. Tour, *ACS Nano* **2014**, *8*, 9518.
- [17] M. R. Gao, W. C. Sheng, Z. B. Zhuang, Q. R. Fang, S. Gu, J. Jiang, Y. S. Yan, *J. Am. Chem. Soc.* **2014**, *136*, 7077.
- [18] Y. Qiu, L. Xin, W. Li, *Langmuir* **2014**, *30*, 7893.
- [19] F. Song, X. Hu, *Nat. Commun.* **2014**, *5*, 4477.
- [20] Z. Y. Li, Z. L. Liu, J. C. Liang, C. W. Xu, X. H. Lu, *J. Mater. Chem. A* **2014**, *2*, 18236.
- [21] S. Q. Ci, S. Mao, Y. Hou, S. M. Cui, H. J. Kim, R. Ren, Z. H. Wen, J. H. Chen, *J. Mater. Chem. A* **2015**, *3*, 7986.
- [22] A. Yamaguchi, R. Inuzuka, T. Takashima, T. Hayashi, K. Hashimoto, R. Nakamura, *Nat. Commun.* **2014**, *5*, 4256.
- [23] L. Trotochaud, J. K. Ranney, K. N. Williams, S. W. Boettcher, *J. Am. Chem. Soc.* **2012**, *134*, 17253.
- [24] D. A. Corrigan, *J. Electrochem. Soc.* **1987**, *134*, 377.
- [25] R. Subbaraman, D. Tripkovic, K. Chang, D. Strmcnik, A. P. Paulikas, P. Hirunsit, M. Chan, J. Greeley, V. Stamenkovic, N. M. Markovic, *Nat. Mater.* **2012**, *11*, 55.
- [26] F. Song, X. Hu, *J. Am. Chem. Soc.* **2014**, *136*, 16481.
- [27] X. Lu, C. Zhao, *Nat. Commun.* **2015**, *6*, 6616.
- [28] Y. Zhao, R. Nakamura, K. Kamiya, S. Nakanishi, K. Hashimoto, *Nat. Commun.* **2013**, *4*, 2390.
- [29] M. Gong, Y. G. Li, H. L. Wang, Y. Y. Liang, J. Z. Wu, J. G. Zhou, J. Wang, T. Regier, F. Wei, H. J. Dai, *J. Am. Chem. Soc.* **2013**, *135*, 8452.
- [30] G. L. Tian, Q. Zhang, B. S. Zhang, Y. G. Jin, J. Q. Huang, D. S. Su, F. Wei, *Adv. Funct. Mater.* **2014**, *24*, 5956.

- [31] S. Chen, J. J. Duan, W. Han, S. Z. Qiao, *Chem. Commun.* **2014**, 50, 207.
- [32] X. Long, J. K. Li, S. Xiao, K. Y. Yan, Z. L. Wang, H. N. Chen, S. H. Yang, *Angew. Chem. Int. Ed.* **2014**, 53, 7584.
- [33] W. Ma, R. Z. Ma, C. X. Wang, J. B. Liang, X. H. Liu, K. C. Zhou, T. Sasaki, *ACS Nano* **2015**, 9, 1977.
- [34] M. X. Li, J. E. Zhu, L. L. Zhang, X. Chen, H. M. Zhang, F. Z. Zhang, S. L. Xu, D. G. Evans, *Nanoscale* **2011**, 3, 4240.
- [35] Y. F. Zhao, S. Q. Chen, B. Sun, D. W. Su, X. D. Huang, H. Liu, Y. M. Yan, K. N. Sun, G. X. Wang, *Sci. Rep.* **2015**, 5, 7629.
- [36] S. Chen, S. Z. Qiao, *ACS Nano* **2013**, 7, 10190.
- [37] S. Chen, J. J. Duan, M. Jaroniec, S. Z. Qiao, *Adv. Mater.* **2014**, 26, 2925.
- [38] G. L. Tian, M. Q. Zhao, D. S. Yu, X. Y. Kong, J. Q. Huang, Q. Zhang, F. Wei, *Small* **2014**, 10, 2251.
- [39] J. Geng, L. Kuai, E. Kan, Q. Wang, B. Y. Geng, *ChemSusChem* **2015**, 8, 659.
- [40] D. Tang, J. Liu, X. Y. Wu, R. H. Liu, X. Han, Y. Z. Han, H. Huang, Y. Liu, Z. H. Kang, *ACS Appl. Mater. Interfaces* **2014**, 6, 7918.
- [41] J. Y. C. Chen, J. T. Miller, J. B. Gerken, S. S. Stahl, *Energy Environ. Sci.* **2014**, 7, 1382.
- [42] A. M. Smith, L. Trotochaud, M. S. Burke, S. W. Boettcher, *Chem. Commun.* **2015**, 51, 5261.
- [43] L. Trotochaud, S. L. Young, J. K. Ranney, S. W. Boettcher, *J. Am. Chem. Soc.* **2014**, 136, 6744.
- [44] D. Friebe, M. W. Louie, M. Bajdich, K. E. Sanwald, Y. Cai, A. M. Wise, M. Cheng, D. Sokaras, T. Weng, R. Alonso-Mori, R. C. Davis, J. R. Bargar, J. K. Nørskov, A. Nilsson, A. T. Bell, *J. Am. Chem. Soc.* **2015**, 137, 1305.
- [45] M. A. Oliver-Tolentino, J. Vázquez-Samperio, A. Manzo-Robledo, R. D. G. González-Huerta, J. L. Flores-Moreno, D. Ramírez-Rosales, A. Guzmán-Vargas, *J. Phys. Chem. C* **2014**, 118, 22432.
- [46] X. W. Yu, M. Zhang, W. J. Yuan, G. Q. Shi, *J. Mater. Chem. A* **2015**, 3, 6921.
- [47] Z. Y. Lu, W. W. Xu, W. Zhu, Q. Yang, X. D. Lei, J. F. Liu, Y. P. Li, X. M. Sun, X. Duan, *Chem. Commun.* **2014**, 50, 6479.
- [48] T. Y. Ma, S. Dai, M. Jaroniec, S. Z. Qiao, *Angew. Chem. Int. Ed.* **2014**, 53, 7281.
- [49] Z. B. Zhuang, W. C. Sheng, Y. Y. Yan, *Adv. Mater.* **2014**, 26, 3950.
- [50] X. M. Zhou, Z. M. Xia, Z. Y. Zhang, Y. Y. Ma, Y. Q. Qu, *J. Mater. Chem. A* **2014**, 2, 11799.
- [51] T. Y. Ma, S. Dai, M. Jaroniec, S. Z. Qiao, *J. Am. Chem. Soc.* **2014**, 136, 13925.
- [52] R. J. Nicholls, A. T. Murdock, J. Tsang, J. Britton, T. J. Pennycook, A. Koós, P. D. Nellist, N. Grobert, J. R. Yates, *ACS Nano* **2013**, 7, 7145.
- [53] S. Chen, J. Duan, J. Ran, M. Jaroniec, S. Z. Qiao, *Energy Environ. Sci.* **2013**, 6, 3693.